Supplementary Information for

Late Pleistocene shrub expansion preceded megafauna turnover and extinctions in eastern Beringia

Alistair J. Monteath [a,b,*], Benjamin V. Gaglioti [c], Mary E. Edwards [b,d] and Duane Froese [a,*]

[a] Department of Earth and Atmospheric Sciences, University of Alberta, Edmonton, Canada
[b] School of Geography and Environmental Science, University of Southampton, Southampton, UK
[c] Water and Environmental Research Center, University of Alaska Fairbanks, Fairbanks, USA
[d] Alaska Quaternary Center, University of Alaska Fairbanks, Fairbanks, USA

Email: ali.monteath@ualberta.ca, duane.froese@ualberta.ca

This DOC file includes:

Supplementary text
Figures S1 to S9
Table S1
SI References

Other supplementary materials for this manuscript include the following:

Supplementary Datasets

Data collection, filtering and interpretation

Lake-sediment records

To assess the chronology of shrub expansion in eastern Beringia, we collated pollen data from online databases (NOAA Climatic Data Center; Neotoma Paleoecology Database) and contributions from the original authors (see *Acknowledgements*). We then examined changes in the abundance of *Salix*, *Betula* and *Alnus*, which, together, represent the dominant shrub taxa present in eastern Beringia during the late Pleistocene (1). Pollen from these taxa is assumed to have been produced by prostrate (e.g. *Salix cf. polaris* and *Salix. cf. arctica*), dwarf (e.g. *Betula nana*) or shrub forms of these plants (e.g. *B. glandulosa*, *S. glauca*) during the late glacial period. Goetcheus and Birks (2) and Zazula et al. (3) report prostrate *Salix* macrofossils of Last Glacial Maximum age (ca. 20 ka): *S. arctica* from Seward Peninsula, and *S*. cf *arctica* and *S*. cf *polaris* macrofossils from the Yukon, respectively. *Salix* and *Betula* macrofossil remains from eastern Beringia in tall-shrub form, along with wood of *Populus*, date from at least 13.5 ka (4).

We only considered the timing of shrub expansion from pollen records where the chronology is based on accelerator mass spectrometer radiocarbon (AMS ^{14}C) dating of terrestrial plant macrofossils. This is because ^{14}C dates from bulk sediments are often inaccurate as they represent the mass-derived mean from a mixture of aquatic and terrestrial organic matter with different ages. This problem is particularly acute at high latitudes, where the combination of eroding lake shorelines, slow rates of organic decomposition and low sediment accumulation rates can result in substantial disagreement (up to several thousand years) between ^{14}C dates derived from plant macrofossils and bulk sediment (5,6,7). This offset is evident in lake records from eastern Beringia that have been dated using both conventional (radiometric) ^{14}C dating and AMS ^{14}C dating, for example: Hanging Lake (8,9), Grandfather Lake (10,11) and Lake of the Pleistocene (7). The type of plant macrofossil remains selected for dating is also important, as aquatic macrofossils may be affected by reservoir effects caused by aquatic plants using dissolved inorganic carbon either from ancient carbonate sources or from respired organic matter (5). It is also known that large pieces of wood and charcoal samples can cause an overestimation of sediment age because they may be stored on the landscape for long periods before deposition (6).

Some studies argue that bulk materials are acceptable in cases where old-carbon inputs to the lake are constant and predictable. In several records, ^{14}C dates from bulk sediment, aquatic macrofossils and terrestrial macrofossils are consistent during the Holocene (where easily dated materials are often more common) suggesting limited effects of old-carbon (e.g. Sunken Island Lake, 12). However, we still excluded these records from this study if the period of shrub expansion was not dated using terrestrial plant macrofossils. This approach was considered necessary as pre-aged terrestrial carbon inputs are not always consistent, particularly during periods of rapid climate change when depositional processes, water tables and thaw rates are likely to have fluctuated (7,13). In summary, delicate macrofossils from terrestrial plants like leaves, seeds, and twigs are the ideal material for assigning a ^{14}C age to a sediment layer and we focus only on lake records that use this reliable dating approach.

Plant macrofossils

We collated a database of ^{14}C dated shrub macrofossils from the relevant published literature (Database S1). We do not differentiate between ^{14}C dates derived from shrub remains identified in growth (*in situ*) or reworked positions as we are concerned with the age of the macrofossil, not the exact location or the association with the host sediment. Radiocarbon-dated macrofossils that were identified as outliers from other dates in the stratigraphic sequence in which they were found by the original authors were excluded from the database as they are likely to be unreliable.

Faunal remains

A database of ^{14}C dated remains from wapiti, moose, bison, horse, mammoth and arctic ground squirrel found in Alaska and Yukon was compiled from the published literature (Database S1). The database is largely composed of dated collagen from megaherbivore bones; however, it also includes arctic ground squirrel middens, which are formed from material that can be reliably ^{14}C dated such as subterranean caches of fruits and seeds, and/or nesting material constructed from the leaves and stems of graminoids (3). We restrict the faunal database to material dated between 20-8 ka, as this time period brackets the regional extinction of mammoth and horse and the extirpation of arctic ground squirrel from large areas of eastern Beringia, as well as the first appearance of moose and expansion of shrub tundra. (1,14,15).

The temporal pattern of arctic ground squirrel and moose remains provide important paleoecological evidence for the demise of the steppe-tundra and expansion of shrub tundra. Modern arctic ground squirrels primarily occupy tundra habitats and were well adapted to the late Pleistocene steppe-tundra. This dry, open habitat maintained deeper active layers than present day, allowing for burrow construction, while helping ground squirrels to visually detect predators (3). Conversely, moose are reliant on tall-shrub vegetation to evade predators and provide winter forage (16). In Alaska the current expansion of Arctic shrub vegetation has been accompanied by a northward extension of moose range (17), where moose exploit increasing tall-shrub habitat availability along river corridors (18). The presence of moose remains can therefore be used to infer the presence of shrub vegetation in a late Pleistocene landscape.

Defining the expansion of shrub tundra in reanalysed pollen records

We define the beginning of shrub tundra expansion as the first sustained increase (replicated in multiple pollen samples) in *Betula* pollen above background values (pre-15 ka). In most records this represents an increase from <5% to >20%, however, there are exceptions to this. At Trout Lake (19), Hanging Lake (9) and Ruppert Lake (20) the expansion of shrub tundra is placed at samples where *Betula* makes up 17-18% of the pollen sum. This approach is justified as in each case the increase of *Betula* is unidirectional, with *Betula* comprising <4% of the pollen sum in the previous sample and >40% in the subsequent one. Therefore, the expansion of shrub tundra was clearly underway at these points.

Okpilak Lake (21), Trout Lake (19), Hanging Lake (9), Lost Lake (22) and Jan Lake (23) all have increases in *Betula* pollen that pre-date the establishment of shrub tundra, defined using the methods above. However, these early increases are all characterised by one unusually high value, that is not replicated, and therefore we do not consider them to be reliable indicators of shrub tundra establishment.

We define the timing of *Salix* expansion as the first sustained increase in *Salix* pollen above background values. In most cases this expansion represents an increase to >15% of the pollen sum; however, the expansion of *Salix* is not as clearly represented as *Betula*. This is because (1) *Salix* had already expanded before lake-sediment began to accumulate in several records, (2) *Salix* produces less pollen than *Betula* and so changes in abundance are not as clear in percentage counts and (3) the expansion of *Salix* is rapidly obscured by expanding *Betula* in many records. We therefore only defined *Salix* expansion five of the 15 records we reanalysed. In Lost Lake (22) we used the larger, later percentage increase in *Salix* pollen (from 12 to 28%) to place the timing of *Salix* expansion ca. 13.8 ka. This timing is consistent with the pollen influx data (Fig. S3), and is unaffected by a large decline in *Cyperaceae* that affects percentage values at the base of the record.

Bayesian age-depth model descriptions

We developed new Bayesian age-depth models for the 15 lake sediment records reanalyzed in this study. For each record (except for Lake of the Pleistocene), we constructed a *P_Sequence* depositional model using OxCal version 4.4 (24,25,26) and the Intcal20 Northern Hemisphere calibration curve (27) (Fig. S1). Boundaries were placed at the contact between depositional units described by the original authors (24). These *P_Sequence* depositional models were run with a general *Outlier Model* and ^{14}C dates were considered for manual rejection when individual agreement indexes fell below 60% (typically caused by an age-reversal) (28).

- Tukuto Lake (29): A *P_Sequence* depositional model was developed from eight ^{14}C dates. One further ^{14}C date was not included in the age-model as it was sampled from below a core break between 299-334 cm depth, and limited chronological information is available below this depth. A boundary was placed at 239 cm depth where sediments changed from inorganic silt to organic silt.

- Okpilak Lake (21): A *P_Sequence* depositional model was developed from 12 ^{14}C dates. Two other ^{14}C dates (CAMS-55826 and CAMS-53243) were removed from the age-depth model as they caused significant age reversals. A boundary was placed at 417 cm depth because of a sharp, prolonged change from inorganic-sediment to gyttja.

- Trout Lake (19): A *P_Sequence* depositional model was developed from nine ^{14}C dates. No stratigraphic description is reported from this core and so no boundaries were used in the age-depth model.

- Hanging Lake (9): A *P_Sequence* depositional model was developed from eight ^{14}C dates. One further ^{14}C date (UCIAMS-20984) was removed from the age-depth model as it caused a significant age reversal. No stratigraphic description is reported from this core and so no boundaries were used in the age-depth model.

- Burial Lake (30): Two *P_Sequence* depositional models were run either side of a hiatus at 340 cm depth using 10 ^{14}C dates. Four further ^{14}C dates (AA-35195, AA-35198, AA-35199 and OS-18369) were removed from the age-depth model as they caused significant age reversals.

- Ruppert Lake (20): A *P_Sequence* depositional model was developed from 10 ^{14}C dates. Three other ^{14}C dates (UCIAMS-139067, SUERC-58892 and SUERC-50487) were removed from the age-depth model as they caused significant age reversals. A cryptotephra deposit derived from the Aniakchak CFE II eruption is present in Ruppert Lake (31), and the age of this event (3.6-3.585 ka BP; 32) was used to further constrain the Ruppert Lake age-depth model. Boundaries were placed at 300 cm and 353 cm depth because of changes in the sediment composition.

- Xindi Lake (33): A *P_Sequence* depositional model was developed from nine ^{14}C dates. One other ^{14}C date (CAMS-105876) was removed from the age-depth model as it caused a significant age reversal. No stratigraphic description is reported from this core and so no boundaries were used in the age-depth model

- Harding Lake (34,35): A *P_Sequence* depositional model was developed from five ^{14}C dates. Two further ^{14}C dates (UCIAMS-109359 and UCIAMS-109360) were excluded from the age-depth model as they caused significant age reversals. Boundaries were placed at contacts between lithogenic units (193 cm, 262 cm, 352 cm and 422 cm depth) inferred from sharp shifts in organic content by the original authors.

- Birch Lake (36): A *P_Sequence* depositional model was developed from eight ^{14}C dates. Two other ^{14}C dates (CAMS-36654 and CAMS-25420) were excluded from the age-depth model as they caused significant age reversals. Boundaries were placed at 1576 cm and 1750 cm depth because of changes in the sediment composition.

- Lost Lake (22): A *P_Sequence* depositional model was developed from five ^{14}C dates. No boundaries were included in this model as placing a boundary at 320 cm depth, where sediments changed from silt to gyttja, resulted in unlikely, high accumulation rates in the lower section or the record.

- Jan Lake (23): A *P_Sequence* depositional model was developed from 18 ^{14}C dates. Four other ^{14}C dates (CAMS-56436, CAMS-48496, CAMS-48497 and CAMS-56444) were excluded from the age-depth model as they caused significant age reversals. A boundary was placed at the base of a core break (133-149 cm depth) during which sediments changed from dense, dry silt to silty gytta with lamina. A tephra deposit derived from the Hayes F2 eruption is present in Jan Lake (31), and the age of this event (4.2-3.9 ka; 32) was used to further constrain the Jan Lake age-depth model.

- Idavain Lake (37): A *P_Sequence* depositional model was developed from 10 ^{14}C dates. Two other dates (CAMS-29159 and CAMS-29162) were removed from the age-depth model as they caused significant age reversals. A boundary was placed at 975 cm depth because of a sharp decrease in clay content and magnetic susceptibility at this depth.

- Beaver Pond (38): A *P_Sequence* depositional model was developed from five ^{14}C dates. Boundaries were placed at 378 cm, 277 cm and 257 cm depth reflecting changes in the sediment composition.

- Discovery Pond (39): A *P_Sequence* depositional model was developed from seven ^{14}C dates. Four other ^{14}C dates (CAMS-113541, CAMS-92754, CAMS-113543 and CAMS-92758) were excluded from the age-depth model as they caused significant age reversals. Boundaries were placed at 398 cm and 358 cm depth because of changes in sediment composition. The age-depth model for Discovery Pond includes ^{14}C dates from three different cores that were placed on a common depth scale by correlating tephra deposits, lithologic boundaries, and magnetic susceptibility (39).

- Lake of the Pleistocene (40): Two ^{14}C dated shrub macrofossils constrain the increase of *Betula* pollen. These were calibrated together using the *Combine* function in Oxcal v.4.4 (25).

AMS ^{14}C dated pollen records excluded from this study

Seven lake sediment records for which AMS ^{14}C dating is available were excluded from this study because of chronological limitations (e.g. unreliable ^{14}C dates at the time of shrub expansion) or insufficient sampling resolution. It is worth noting that three of these sites: Sunken Island Lake (12), Windmill Lake (41) and Grandfather Lake (10,11), place the onset of *Betula* expansion during the early Bølling–Allerød chronozone, in agreement with the re-analyzed AMS ^{14}C dated lake sediment records included in this study. Pollen data from two further lakes, Nimgun Lake (42) and Arolik Lake (43), were unavailable at the time of data compilation.

- Sunken Island Lake (12): The basal ^{14}C date from Sunken Island Lake (UCIAMS-69755), which is the only ^{14}C date from the Bølling–Allerød chronozone in this record, was made on aquatic macrofossils (algal copropel) and so may be contaminated with old-carbon.

- Windmill Lake (41): The chronology for Windmill Lake is largely developed from aquatic macrofossils.

- Trout Lake (44): The pollen sampling resolution (65-25 cm across the late Pleistocene) from Trout Lake is insufficient to accurately determine the timing of shrub expansion.

- Ruppert Lake (33): Although the chronology of Ruppert Lake is well established throughout the Holocene, the pollen evidence for shrub expansion occurs 23 cm below the oldest ^{14}C date from the analyzed sediment core and around 1000 years later (determined by extrapolation) than the *Betula* rise reported from Ruppert Lake by McGowan et al. (20). Given the limited chronological control at the point of shrub expansion, and agreement between the McGowan et al. (20) age-depth model and Xindi Lake age-depth model (33) (which is closely situated to Ruppert Lake), we consider the Higuera et al (33) Ruppert Lake age-depth model unreliable at the point of shrub expansion.

- Grandfather Lake (10,11): The basal ^{14}C date from Grandfather Lake (Beta-59071), which is the only ^{14}C date from the Bølling–Allerød chronozone, was made on bulk sediment and so may be contaminated with old-carbon.

- Antifreeze Pond and Eikland Pond (45): The original authors noted rapid influxes of inorganic material in these records during the late Pleistocene (between 16-11 ka), which they suggested was washed, slumped or blown into the ponds from surrounding loessic soils. The late Pleistocene environmental record was therefore considered unreliable by the original authors.

Figures and Tables

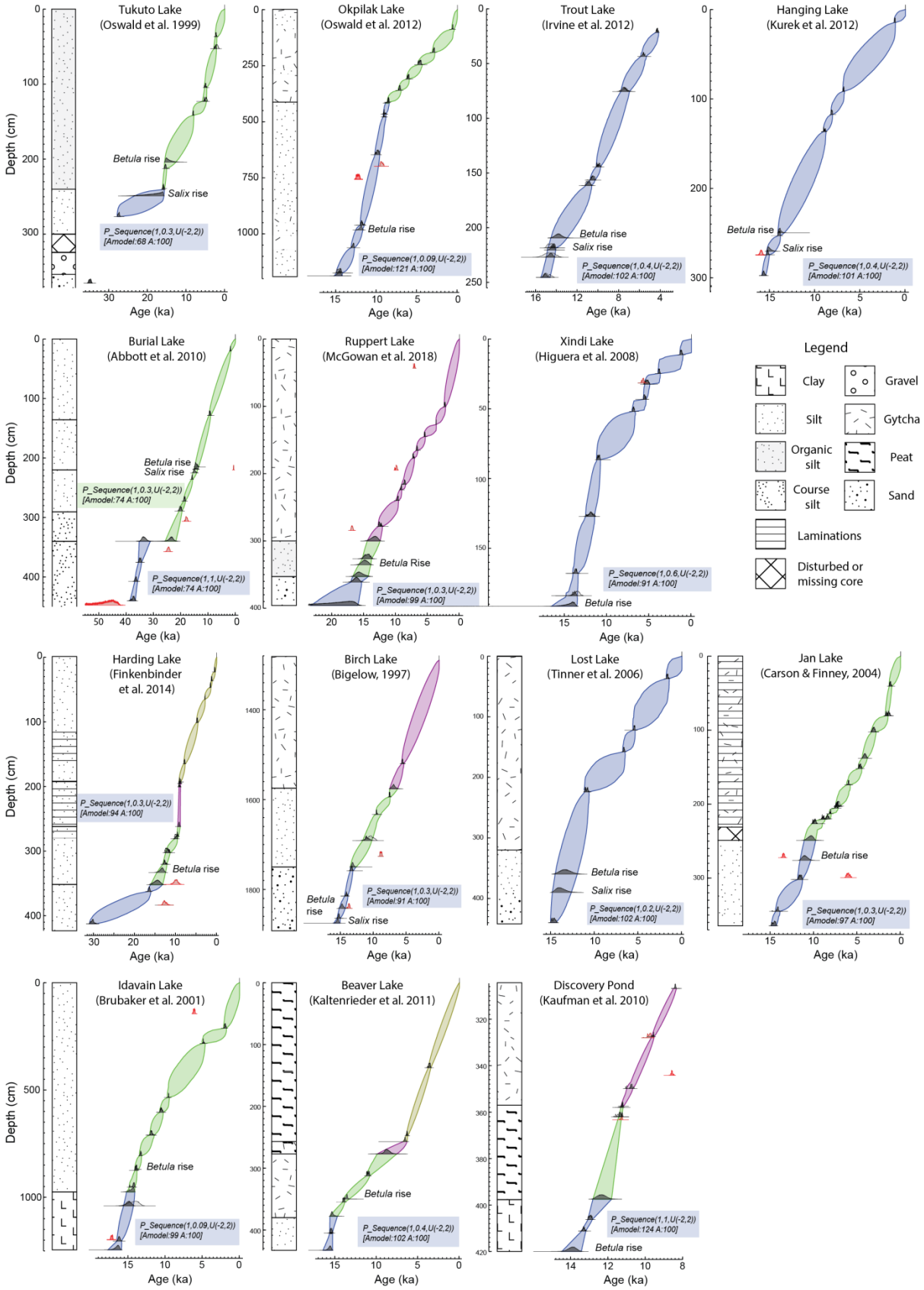

Fig. S1. Bayesian age-depth models and stratigraphic logs from reanalyzed AMS ^{14}C dated records in eastern Beringia. Stratigraphic logs were drawn from sediment descriptions made by the original authors. Outlier ^{14}C dates are shown in red and boundaries between sediment units are indicated by colour changes in the modelled two sigma age-ranges.

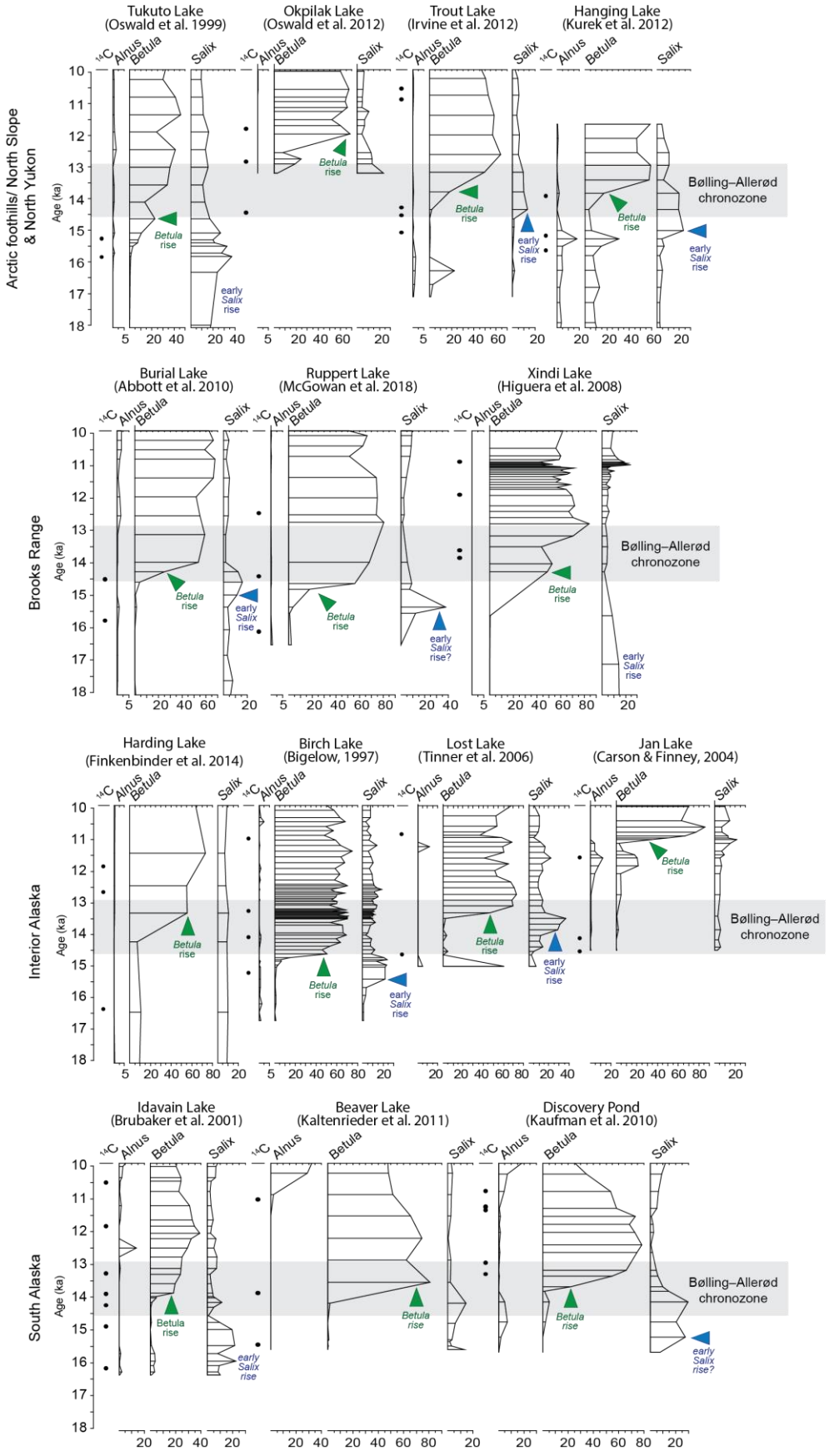

Fig. S2. Pollen percentage profiles from reanalyzed AMS ^{14}C dated records in eastern Beringia. The median of calibrated age ranges from ^{14}C dates are indicated by black circles. The Bølling–Allerød chronozone is placed between 14.6-12.9 ka (46).

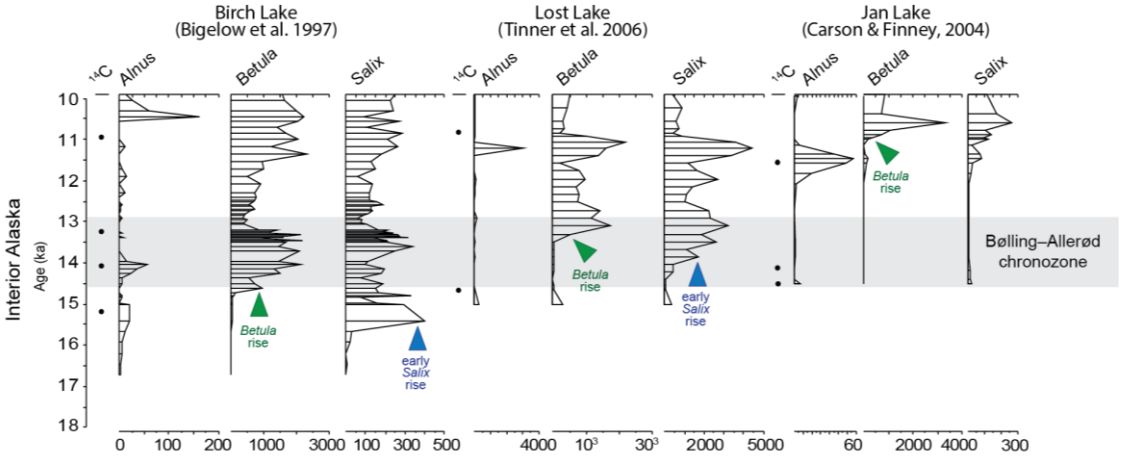

Fig. S3. Pollen influx profiles (grains cm^{-2} yr^{-1}) from reanalyzed AMS ^{14}C dated records in eastern Beringia. The median of age ranges from calibrated ^{14}C dates are indicated by black circles. The Bølling–Allerød chronozone is placed between 14.6-12.9 ka (46).

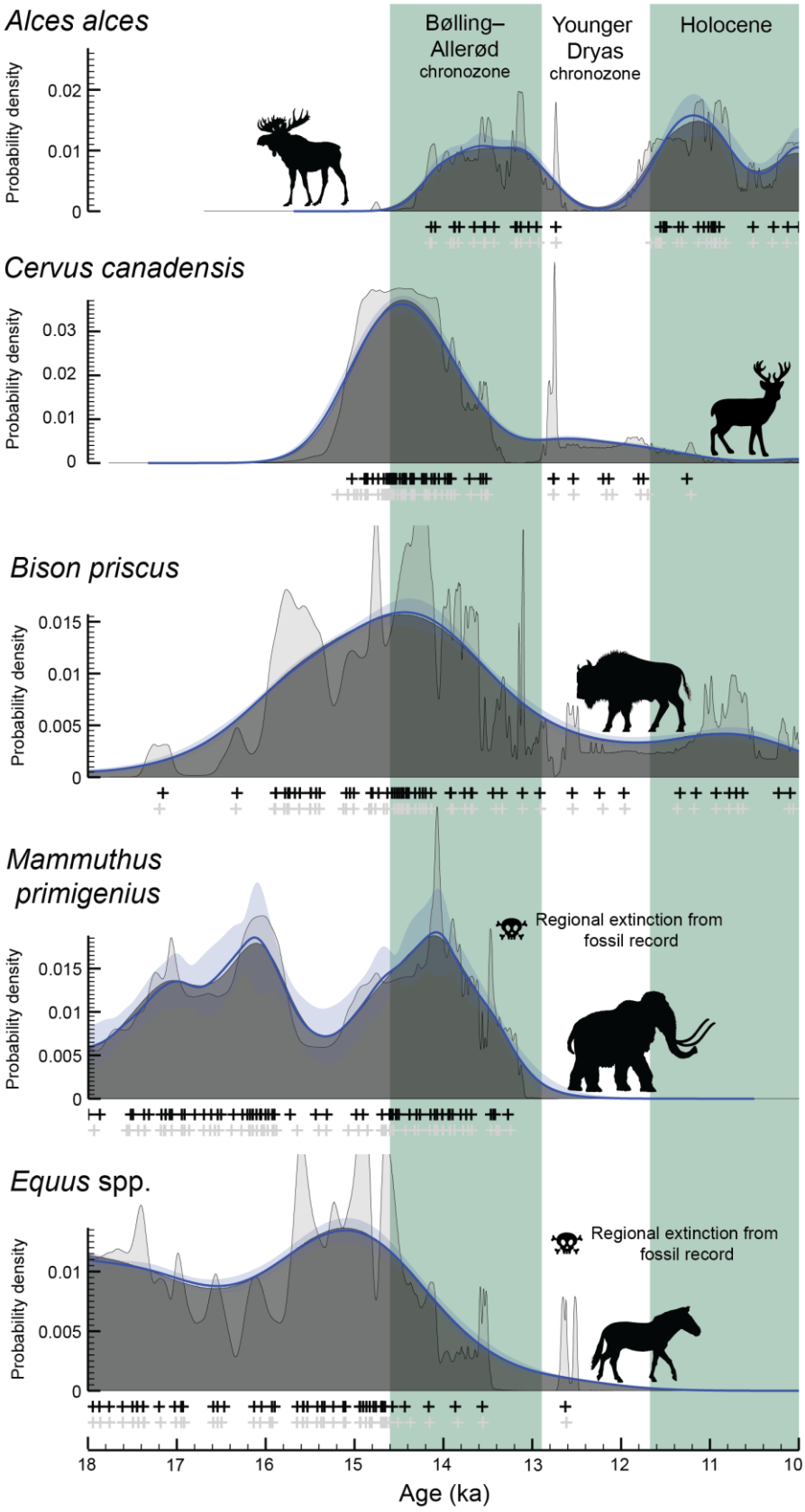

Fig. S4. Posterior distributions and Oxcal *KDE_Model* outputs for megafauna in eastern Beringia (47). The mean and ±1σ of the KDE distributions from the MCMC analysis are show as blue lines and shading. The dark grey shading indicates the sampled kernel density estimation distribution and the light grey shading shows the sum distribution. Light gray crosses indicate the median likelihoods of the calibrated ^{14}C dates, and black crosses show the median of the marginal posterior distributions.

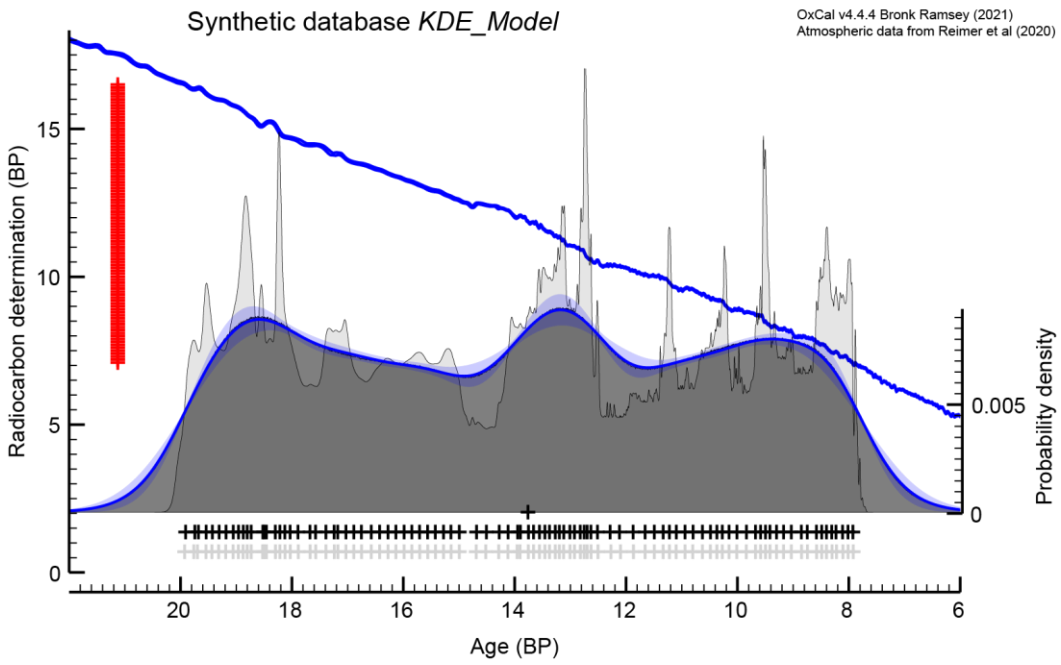

Fig. S5. Posterior distributions and Oxcal *KDE_Model* outputs for the synthetic ^{14}C database (47), shown with the Intcal20 Northern Hemisphere calibration curve (27). The mean and ±1σ of the KDE distributions from the MCMC analysis are shown as blue lines and shading. The dark grey shading indicates the sampled kernel density estimation distribution and the light grey shading shows the sum distribution. Light gray crosses indicate the median likelihoods of the calibrated ^{14}C dates, and black crosses show the median of the marginal posterior distributions. The Intcal20 calibration curve (27) is show above the *KDE_Model* outputs as a blue band and the central values of the simulated ^{14}C dates are shown in red.

Tukuto Lake

```
Plot()
 {
  Outlier_Model("General",T(5),U(0,4),"t");
  P_Sequence("",1,0.3,U(-2,2))
  {
   Boundary();
   R_Date("CAMS-44176",30410,300)
   {
    color="red";
    Outlier();
    Outlier(0.05);
    z=365.5;
   };
   R_Date("CAMS-44175",23050,220)
   {
    Outlier(0.05);
    z=276.5;
   };
   Date("Salix Rise")
   {
    z=249;
   };
   R_Date("CAMS-42615",13190,60)
   {
    Outlier(0.05);
    z=240.5;
   };
   Boundary()
   {
    z=239;
   };
   R_Date("CAMS-42614",12830,100)
   {
    Outlier(0.05);
    z=212.5;
   };
   Date("Betula rise")
   {
    z=204;
   };
   R_Date("CAMS-44174",7280,50)
   {
    Outlier(0.05);
    z=141.5;
   };
   R_Date("CAMS-42613",4250,140)
   {
    Outlier(0.05);
    z=123;
   };
   R_Date("CAMS-44173",4350,90)
   {
    Outlier(0.05);
    z=104.5;
   };
   R_Date("CAMS-42612",2030,240)
   {
    Outlier(0.05);
    z=53;
   };
   R_Date("CAMS-44172",2240,80)
   {
    Outlier(0.05);
    z=37;
   };
   Date("Top",N(1996))
   {
    z=0;
   };
   Boundary();
  };
 };
```

Okpilak Lake

```
Plot()
 {
  Outlier_Model("General",T(5),U(0,4),"t");
  P_Sequence("",1,0.09,U(-2,2))
  {
   Boundary()
   {
    z=1187;
   };
   R_Date("CAMS-69506",12430,50)
   {
    Outlier(0.05);
    z=1174.5;
   };
   Date("Betula rise")
   {
    z=1068;
   };
   R_Date("CAMS-51449",10870,110)
   {
    Outlier(0.05);
    z=1062;
   };
   R_Date("CAMS-51448",10140,50)
   {
    Outlier(0.05);
    z=961.5;
   };
   R_Date("CAMS-53243",10370,50)
   {
    Outlier();
    Outlier(0.05);
    z=756.5;
   };
   R_Date("CAMS-55826",8350,130)
   {
    Outlier();
    Outlier(0.05);
    z=698.5;
   };
   R_Date("CAMS-57064",8770,80)
   {
    Outlier(0.05);
    z=646.5;
   };
   R_Date("CAMS-76815",8090,40)
   {
    Outlier(0.05);
    z=478.5;
   };
   R_Date("CAMS-51447",8080,50)
   {
    Outlier(0.05);
    z=466;
   };
   Boundary()
   {
    z=417;
   };
   R_Date("CAMS-53242",7680,60)
   {
    Outlier(0.05);
    z=412.5;
   };
   R_Date("CAMS-57065",6180,50)
   {
    Outlier(0.05);
    z=359.5;
   };
   R_Date("CAMS-53241",5240,50)
   {
    Outlier(0.05);
    z=309;
   };
   R_Date("CAMS-53240",4070,80)
   {
    Outlier(0.05);
    z=245.5;
   };
   R_Date("CAMS-51446",2750,60)
   {
    Outlier(0.05);
    z=190.5;
   };
   R_Date("CAMS-57063",480,50)
   {
    Outlier(0.05);
    z=87;
   };
   Date("Top",N(1997))
   {
    z=0;
   };
   Boundary();
  };
 };
```

Trout Lake

```
Plot()
 {
  Outlier_Model("General",T(5),U(0,4),"t");
  P_Sequence("",1,0.4,U(-2,2))
  {
   Boundary()
   {
   };
   R_Date("UCIAMS-37860",12580,120)
   {
    Outlier(0.05);
    z=245.5;
   };
   R_Date("UCIAMS-37859",12430,310)
   {
    Outlier(0.05);
    z=227;
   };
   Date("Salix rise")
   {
    z=220.5;
   };
   R_Date("UCIAMS-37858",12410,100)
   {
    Outlier(0.05);
    z=218.5;
   };
   Date("Betula Rise")
   {
    z=209.5;
   };
   R_Date("UCIAMS-37857",9610,100)
   {
    Outlier(0.05);
    z=161.5;
   };
   R_Date("UCIAMS-37856",9280,100)
   {
    Outlier(0.05);
    z=156.5;
   };
   R_Date("UCIAMS-24252",8835,35)
   {
    Outlier(0.05);
    z=144.5;
   };
   R_Date("UCIAMS-24251",6640,210)
   {
    Outlier(0.05);
    z=75.5;
   };
   R_Date("UCIAMS-37855",4880,80)
   {
    Outlier(0.05);
    z=43.5;
   };
   R_Date("UCIAMS-24250",3860,20)
   {
    Outlier(0.05);
    z=21.5;
   };
   Boundary();
  };
 };
```

Hanging Lake

```
Plot()
 {
  Outlier_Model("General",T(5),U(0,4),"t");
  P_Sequence("",1,0.4,U(-2,2))
  {
   Boundary()
   {
   };
   R_Date("UCIAMS-37860",12580,120)
   {
    Outlier(0.05);
    z=245.5;
   };
   R_Date("UCIAMS-37859",12430,310)
   {
    Outlier(0.05);
    z=227;
   };
   Date("Salix rise")
   {
    z=220.5;
   };
   R_Date("UCIAMS-37858",12410,100)
   {
    Outlier(0.05);
    z=218.5;
   };
   Date("Betula Rise")
   {
    z=209.5;
   };
   R_Date("UCIAMS-37857",9610,100)
   {
    Outlier(0.05);
    z=161.5;
   };
   R_Date("UCIAMS-37856",9280,100)
   {
    Outlier(0.05);
    z=156.5;
   };
   R_Date("UCIAMS-24252",8835,35)
   {
    Outlier(0.05);
    z=144.5;
   };
   R_Date("UCIAMS-24251",6640,210)
   {
    Outlier(0.05);
    z=75.5;
   };
   R_Date("UCIAMS-37855",4880,80)
   {
    Outlier(0.05);
    z=43.5;
   };
   R_Date("UCIAMS-24250",3860,20)
   {
    Outlier(0.05);
    z=21.5;
   };
   Boundary();
  };
 };
```

Fig. S6. Oxcal code for Bayesian age-depth models from Tukuto Lake (29), Okpilak Lake (21), Trout Lake (19) and Hanging Lake (9).

Burial Lake

```
Plot()
 {
  Outlier_Model("General",T(5),U(0,4),"t");
  P_Sequence("",1,1,U(-2,2))
  {
   Boundary();
   R_Date("OS-18369",42600,2800)
   {
    Outlier();
    Outlier(0.05);
    z=447.5;
   };
   R_Date("OS-27279",32780,280)
   {
    Outlier(0.05);
    z=440;
   };
   R_Combine("CAMS-73175/CAMS-73174")
   {
    R_Date("CAMS-73175",32770,470);
    R_Date("CAMS-73174",31680,360);
    Outlier(0.05);
    z=407.5;
   };
   R_Date("OS-18368",30300,300)
   {
    Outlier(0.05);
    z=375.5;
   };
   R_Date("AA-35199",20330,280)
   {
    Outlier();
    Outlier(0.05);
    z=357.5;
   };
   Boundary()
   {
    z=340;
   };
  };
  Outlier_Model("General",T(5),U(0,4),"t");
  P_Sequence("",1,0.3,U(-2,2))
  {
   Boundary()
   {
    z=340;
   };
   R_Date("AA-35198",14660,250)
   {
    Outlier();
    Outlier(0.05);
    z=306.5;
   };
   R_Date("CAMS-73173",16740,260)
   {
    Outlier(0.05);
    z=289;
   };
   R_Date("OS-18367",15300,180)
   {
    Outlier(0.05);
    z=272.5;
   };
   R_Date("OS-17700",13150,65)
   {
    Outlier(0.05);
    z=236;
   };
   Date("Salix rise")
   {
    z=225;
   };
   R_Date("AA-35195",640,85)
   {
    Outlier();
    Outlier(0.05);
    z=220;
   };
   R_Date("CAMS-73172",12020,190)
   {
    Outlier(0.05);
    z=219;
   };
     Date("Betula rise")
   {
    z=215;
   };
   R_Date("AA-35197",8390,140)
   {
    Outlier(0.05);
    z=128.5;
   };
   R_Date("OS-18365",1850,55)
   {
    Outlier(0.05);
    z=20;
   };
   Date("Top",N(2006))
   {
    z=0;
   };
   Boundary()
   {
   };
  };
};
```

Ruppert Lake

```
Plot()
 {
  Outlier_Model("General",T(5),U(0,4),"t");
  P_Sequence("",1,0.3,U(-2,2))
  {
   Boundary()
   {
    z=396;
   };
   R_Date("UCIAMS-154527",13410,270)
   {
    Outlier(0.05);
    z=361;
   };
   Boundary()
   {
    z=341.5;
   };
   Date("Betula Rise")
   {
    z=335.5;
   };
   R_Date("UCIAMS-172052",12290,260)
   {
    Outlier(0.05);
    z=326.5;
   };
   Boundary()
   {
    z=300;
   };
   R_Date("SUERC-50487",13837,59)
   {
    Outlier();
    Outlier(0.05);
    z=284.5;
   };
   R_Date("UCIAMS-154529",10500,70)
   {
    Outlier(0.05);
    z=278.5;
   };
   R_Date("UCIAMS-164418",8650,60)
   {
    Outlier(0.05);
    z=240;
   };
   R_Date("UCIAMS-154510",8145,35)
   {
    Outlier(0.05);
    z=224;
   };
   R_Date("UCIAMS-164417",7760,70)
   {
    Outlier(0.05);
    z=216;
   };
   R_Date("SUERC-58892",8806,43)
   {
    Outlier();
    Outlier(0.05);
    z=195;
   };
   R_Date("UCIAMS-154509",6250,30)
   {
    Outlier(0.05);
    z=177;
   };
   R_Date("UCIAMS-139068",5790,35)
   {
    Outlier(0.05);
    z=165.5;
   };
   R_Date("UCIAMS-164425",4635,25)
   {
    Outlier(0.05);
    z=145;
   };
   Date("Aniakchak CFE II",N(calBP(3593),8))
   {
    z=127;
   };
   R_Date("UCIAMS-154508",2200,25)
   {
    Outlier(0.05);
    z=100.5;
   };
   R_Date("UCIAMS-139067 ",6125,35)
   {
    Outlier();
    Outlier(0.05);
    z=43.5;
   };
   Date("Top",N(2013))
   {
    z=0;
   };
   Boundary();
  };
};
```

Xindi Lake

```
Plot()
 {
  Outlier_Model("General",T(5),U(0,4),"t");
  P_Sequence("",1,0.6,U(-2,2))
  {
   Boundary();
    };
   Date("Betula rise")
   {
    z=191.5;
   };
   R_Date("CAMS-114333",11570,300)
   {
    Outlier(0.05);
    z=184;
   };
   R_Date("CAMS-114332",11800,120)
   {
    Outlier(0.05);
    z=168;
   };
   R_Date("CAMS-114331",10180,120)
   {
    Outlier(0.05);
    z=127.25;
   };
   R_Date("CAMS-106159",9585,40)
   {
    Outlier(0.05);
    z=86.5;
   };
   R_Date("CAMS-116227",5960,60)
   {
    Outlier(0.05);
    z=52;
   };
   R_Date("CAMS-113559",4760,70)
   {
    Outlier(0.05);
    z=43.25;
   };
   R_Date("CAMS-112145",4560,120)
   {
    Outlier(0.05);
    z=32.5;
   };
   R_Date("CAMS-105876",4930,90)
   {
    Outlier();
    Outlier(0.05);
    z=31.5;
   };
   R_Date("CAMS-116226",3490,35)
   {
    Outlier(0.05);
    z=24.75;
   };
   R_Date("CAMS-113558",1240,70)
   {
    Outlier(0.05);
    z=11.25;
   };
   Date("Top",N(2003))
   {
    z=0;
   };
   Boundary();
  };
};
```

Fig. S7. Oxcal code for Bayesian age-depth models from Burial Lake (30), Ruppert Lake (20) and Xindi Lake (33).

Harding Lake

```
Plot()
 {
  Outlier_Model("General",T(5),U(0,4),"t");
  P_Sequence("",1,0.3,U(-2,2))
  {
   Boundary();
   R_Date("89213",25900,320)
   {
    Outlier(0.05);
    z=412.5;
   };
   R_Date("109360",10740,310)
   {
    Outlier();
    Outlier(0.05);
    z=383.5;
   };
   R_Date("89212",13560,100)
   {
    Outlier(0.05);
    z=362.5;
   };
   Boundary()
   {
    z=352;
   };
   R_Date("109359",8770,370)
   {
    Outlier();
    Outlier(0.05);
    z=351.5;
   };
    Date("Betula rise")
   {
    z=333;
   };
   R_Date("109358",10690,190)
   {
    Outlier(0.05);
    z=320.5;
   };
   R_Date("109357",10310,160)
   {
    Outlier(0.05);
    z=302.5;
   };
   R_Date("89211",8820,160)
   {
    Outlier(0.05);
    z=281;
   };
   R_Date("89210",8450,80)
   {
    Outlier(0.05);
    z=277.5;
   };
   Boundary()
   {
    z=262;
   };
   R_Date("89209",8130,60)
   {
    Outlier(0.05);
    z=200.5;
   };
   R_Date("89208",8000,100)
   {
    Outlier(0.05);
    z=195.5;
   };
   Boundary()
   {
    z=193;
   };
   R_Date("89207",6960,70)
   {
    Outlier(0.05);
    z=165;
   };
   R_Date("89206",4160,45)
   {
    Outlier(0.05);
    z=101;
   };
   R_Date("89205",2700,15)
   {
    Outlier(0.05);
    z=65;
   };
   R_Date("89204",1570,40)
   {
    Outlier(0.05);
    z=46.5;
   };
   R_Date("109356",1245,25)
   {
    Outlier(0.05);
    z=36.5;
   };
   R_Date("89203",380,30)
   {
    Outlier(0.05);
    z=22.5;
   };
   Date("Top",N(2010))
   {
    z=0;
   };
   Boundary();
  };
 };
```

Birch Lake

```
Plot()
 {
  Outlier_Model("General",T(5),U(0,4),"t");
  P_Sequence("",1,0.3,U(-2,2))
  {
   Boundary();
    };
   Date("Salix rise")
   {
    z=1875;
   };
   R_Date("CAMS-25421",12780,60)
   {
    Outlier(0.05);
    z=1864;
   };
   R_Date("CAMS-25420",11840,100)
   {
    Outlier();
    Outlier(0.05);
    z=1842;
    };
   Date("Betula Rise")
   {
    z=1837;
   };
   R_Date("CAMS-36655",12150,70)
   {
    Outlier(0.05);
    z=1815;
   };
   R_Date("CAMS-25424",11420,120)
   {
    Outlier(0.05);
    z=1758.5;
   };
   Boundary()
   {
    z=1750;
   };
   R_Date("CAMS-36654",7950,50)
   {
    Outlier();
    Outlier(0.05);
    z=1726.25;
   };
   R_Date("CAMS-25423",9210,340)
   {
    Outlier(0.05);
    z=1691;
   };
   R_Date("CAMS-25427",8480,60)
   {
    Outlier(0.05);
    z=1633;
   };
   R_Combine("CAMS-25422/CAMS-25425")
   {
    R_Date("CAMS-25422",6630,90);
    R_Date("CAMS-25425",6590,60);
    Outlier(0.05);
    z=1594;
   };
   Boundary()
   {
    z=1576;
   };
   R_Date("CAMS-25425",4810,60)
   {
    Outlier(0.05);
    z=1520;
   };
   Date("Top",N(1994))
   {
    z=1290;
   };
   Boundary();
  };
 };
```

Jan Lake

```
Plot()
 {
  Outlier_Model("General",T(5),U(0,4),"t");
  P_Sequence("",1,0.3,U(-2,2))
  {
   Boundary();
   R_Combine("CAMS-48498/CAMS-58299")
   {
    R_Date("CAMS-48498",12430,40);
    R_Date("CAMS-58299",12410,50);
    Outlier(0.05);
    z=364.5;
   };
   R_Date("CAMS-16066",12220,70)
   {
    Outlier(0.05);
    z=345;
   };
   R_Date("CAMS-56445",10010,60)
   {
    Outlier(0.05);
    z=302;
   };
   R_Date("CAMS-56444",22180,140)
   {
    Outlier();
    Outlier(0.05);
    z=300;
   };
   R_Date("CAMS-48497",5220,150)
   {
    Outlier();
    Outlier(0.05);
    z=299.5;
    };
   Date("Betula rise")
   {
    z=276;
   };
   R_Date("CAMS-48496",11590,100)
   {
    Outlier();
    Outlier(0.05);
    z=272.5;
   };
   Boundary()
   {
    z=249;
   };
   R_Date("CAMS-39082",8830,50)
   {
    Outlier(0.05);
    z=226.5;
   };
   R_Date("CAMS-56443", 8050, 50)
   {
    Outlier(0.05);
    z=220.5;
   };
   R_Date("CAMS-56442", 7570, 100)
   {
    Outlier(0.05);
    z=220;
   };
   R_Combine("CAMS-56441/CAMS-56440")
   {
    R_Date("CAMS-56441",7220,40);
    R_Date("CAMS-56440",7260,50);
    Outlier(0.05);
    z=213;
   };
   R_Date("CAMS-39081",6500,100)
   {
    Outlier(0.05);
    z=205.5;
   };
   R_Date("CAMS-39080",6360,90)
   {
    Outlier(0.05);
    z=203.5;
   };
   R_Date("CAMS-39079",6230,100)
   {
    Outlier(0.05);
    z=202.5;
   };
   R_Combine("CAMS-56439/CAMS-56438")
   {
    R_Date("CAMS-56439",5220,50);
    R_Date("CAMS-56438",5000,110);
    Outlier(0.05);
    z=174;
   };
   R_Date("CAMS-16065",4100,50)
   {
    Outlier(0.05);
    z=152;
   };
```

Lost Lake

```
Plot()
 {
  Outlier_Model("General",T(5),U(0,4),"t");
  P_Sequence("",1,0.2,U(-2,2))
  {
   Boundary()
   {
   };
   R_Date("CAMS-68674",12460,50)
   {
    Outlier(0.05);
    z=440;
   };
     Date("Salix rise")
   {
    z=390;
    };
   Date("Betula Rise")
   {
    z=360;
   };
   R_Date("CAMS-68675",9530,50)
   {
    Outlier(0.05);
    z=224;
   };
   R_Date("CAMS-68676",5800,40)
   {
    Outlier(0.05);
    z=158;
   };
   R_Date("CAMS-68677",4670,40)
   {
    Outlier(0.05);
    z=122;
   };
   R_Date("CAMS-68678",1710,60)
   {
    Outlier(0.05);
    z=37;
   };
   Date("Top",N(2000))
   {
    z=0;
   };
   Boundary();
  };
 };
```

Jan Lake (continued)

```
Date("Hayes F2",N(calBP(4058),148))
   {
    z=138;
   };
   R_Date("CAMS-48495",2920,90)
   {
    Outlier(0.05);
    z=102.5;
   };
   R_Date("CAMS-56437", 1650, 50)
   {
    Outlier(0.05);
    z=80.5;
   };
   R_Date("CAMS-56436", 1400, 100)
   {
    Outlier();
    Outlier(0.05);
    z=80.5;
   };
   R_Date("CAMS-56435",1220,50)
   {
    Outlier(0.05);
    z=40.5;
   };
   Date("Top",N(1994))
   {
    z=0;
   };
   Boundary();
  };
 };
```

Fig. S8. Oxcal code for Bayesian age-depth models from Harding Lake (34), Birch Lake (36), Jan Lake (23) and Lost Lake (22).

Idavain Lake

```
Plot()
 {
  Outlier_Model("General",T(5),U(0,4),"t");
  P_Sequence("",1,0.09,U(-2,2))
  {
   Boundary()
   {
    z=1245;
   };
   R_Date("CAMS-30330",13440,90)
   {
    Outlier(0.05);
    z=1204.5;
   };
   R_Date("CAMS-29162",14100,60)
   {
    Outlier();
    Outlier(0.05);
    z=1197.5;
   };
   R_Date("Beta-6156",12070,490)
   {
    Outlier(0.05);
    z=1040;
   };
   Boundary()
   {
    z=975;
   };
   R_Date("CAMS-26229",12280,60)
   {
    Outlier(0.05);
    z=953;
   };
    R_Date("CAMS-18371",12050,70)
   {
    Outlier(0.05);
    z=875;
   };
   Date("Betula Rise")
   {
    z=870;
   };
   R_Date("CAMS-26228",11410,60)
   {
    Outlier(0.05);
    z=806.5;
   };
   R_Date("CAMS-26227",10180,60)
   {
    Outlier(0.05);
    z=710.5;
   };
   R_Date("CAMS-26226",9320,80)
   {
    Outlier(0.05);
    z=604;
   };
   R_Date("CAMS-18372",8540,60)
   {
    Outlier(0.05);
    z=535;
   };
   R_Date("CAMS-29161",4270,50)
   {
    Outlier(0.05);
    z=283.5;
   };
   R_Date("CAMS-29160",1960,60)
   {
    Outlier(0.05);
    z=212.5;
   };
   R_Date("CAMS-29159",5280,60)
   {
    Outlier();
    Outlier(0.05);
    z=144.5;
   };
   Date("Top",N(1998))
   {
    z=0;
   };
   Boundary();
  };
 };
```

Beaver Lake

```
Plot()
 {
  Outlier_Model("General",T(5),U(0,4),"t");
  P_Sequence("",1,0.4,U(-2,2))
  {
   Boundary()
   {
    z=433;
   };
   R_Date("LLNL-62023",12890,50)
   {
    Outlier(0.05);
    z=405;
   };
   Boundary()
   {
    z=378;
   };
   Date("Salix rise")
   {
    z=360;
   };
   R_Date("LLNL-59807",12050,50)
   {
    Outlier(0.05);
    z=355;
   };
   Date("Betula Rise")
   {
    z=350;
   };
   R_Date("LLNL-62024",9620,50)
   {
    Outlier(0.05);
    z=312.5;
   };
   Boundary()
   {
    z=277;
   };
   Boundary()
   {
    z=257;
   };
   R_Date("LLNL-59808",5470,50)
   {
    Outlier(0.05);
    z=247.5;
   };
   R_Date("LLNL-59809",3350,80)
   {
    Outlier(0.05);
    z=137.5;
   };
   Date("Top",N(1991))
   {
    z=0;
   };
   Boundary();
  };
 };
```

Discovery Pond

```
Plot()
 {
  Outlier_Model("General",T(5),U(0,4),"t");
  P_Sequence("",1,1,U(-2,2))
  {
   Boundary();

   Date("Betula Rise")
   {
    z=420;
   };
   R_Date("CAMS-113544",11435,40)
   {
    Outlier(0.05);
    z=411.2;
   };
   R_Date("CAMS-92759",11015,35)
   {
    Outlier(0.05);
    z=406.3;
   };
   Boundary()
   {
    z=397.5;
   };
   R_Date("CAMS-113543",9865,40)
   {
    Outlier();
    Outlier(0.05);
    z=363.3;
   };
   R_Date("CAMS-92758", 9835, 35)
   {
    Outlier();
    Outlier(0.05);
    z=362;
   };
   R_Date("CAMS-92757", 9970, 30)
   {
    Outlier(0.05);
    z=362;
   };
   R_Date("CAMS-92754",9845,45)
   {
    Outlier(0.05);
    z=358;
   };
   Boundary()
   {
    z=357.5;
   };
   R_Date("CAMS-113542",9485,35)
   {
    Outlier(0.05);
    z=349.9;
   };
   R_Date("CAMS-113541",7795,40)
   {
    Outlier();
    Outlier(0.05);
    z=344.2;
   };
   R_Date("CAMS-92756", 8760, 35)
   {
    Outlier();
    Outlier(0.05);
    z=328;
   };
   R_Date("CAMS-92755", 8620, 35)
   {
    Outlier(0.05);
    z=327.5;
   };
   R_Date("CAMS-113540",7585,45)
   {
    Outlier(0.05);
    z=306.8;
   };
   Boundary();
  };
 };
```

Fig. S9. Oxcal code for Bayesian age-depth models from Idavain Lake (37), Beaver Lake (38) and Discovery Pond (39).

Table S1. Modelled age ranges for different defined shrub expansion depths. (1) The first sustained increase as used in this study. (2) Last steppe-tundra sample refers to the pollen sample immediately beneath the first sustained increase in Betula. (3) The modelled age range for a sediment depth taken at the mid-point between the first sustained increase and last steppe-tundra samples.

Salix

Site/ref	(1) First sustained increase			(2) Last steppe-tundra sample			(3) Middle depth		
	Depth (cm)	Mean (ka)	2σ range (ka)	Depth (cm)	Mean (ka)	2σ range (ka)	Depth (cm)	Mean (ka)	2σ range (ka)
Burial Lake (30)	225	14.99	15.51-14.10	230	15.37	15.82-14.654	227.5	15.18	15.70-14.35
Tukuto Lake (29)	*Salix* is abundant from the lowermost sample								
Lake of the Pleistocene (40)	-	-	-	-	-	-	-	-	-
Okpilak Lake (21)	*Salix* is abundant from the lowermost sample								
Trout Lake (19)	220.5	14.35	14.85-14.06	230.5	14.64	15.05-14.25	225.5	14.49	14.92-14.15
Hanging Lake (9)	270.75	15.01	15.31-14.40	280.25	15.28	15.55-15.07	275.5	15.19	15.37-15.02
Ruppert Lake (20)	*Salix* rise quickly obscured by *Betula* rise								
Xindi Lake (33)	*Salix* is abundant from the lowermost sample								
Harding Lake (34)	*Salix* is abundant from the lowermost sample								
Birch Lake (36)	1875	15.41	16.01-15.07	1885	15.67	16.28-15.33	1880	15.51	16.19-15.12
Lost Lake (22)	390	13.86	14.80-12.63	400	14.05	14.86-12.88	395	13.95	14.80-12.79
Jan Lake (23)	No clear *Salix* rise								
Idavain Lake (37)	*Salix* is abundant from the lowermost sample								
Beaver Lake (38)	*Salix* rise quickly obscured by *Betula* rise								
Discovery Pond (39)	*Salix* is abundant from the lowermost sample								

Betula

Site/ref	(1) First sustained increase			(2) Last steppe-tundra sample			(3) Middle depth		
	Depth (cm)	Mean (ka)	2σ range (ka)	Depth (cm)	Mean (ka)	2σ range (ka)	Depth (cm)	Mean (ka)	2σ range (ka)
Burial Lake (30)	215	14.28	14.84-13.47	220	14.60	15.08-13.80	217.5	14.43	14.93-13.65
Tukuto Lake (29)	204	14.64	15.53-12.62	209	15.09	15.60-13.69	206.5	14.88	15.57-12.98
Lake of the Pleistocene (40)	-	-	-	-	-	-	-	-	-
Okpilak Lake (21)	980	11.95	12.46-11.63	1030	12.54	12.95-12.02	1005	12.24	12.76-11.78
Trout Lake (19)	209.5	13.79	14.53-12.96	220.5	14.35	14.85-14.06	215	14.11	14.68-13.47
Hanging Lake (9)	249.75	13.83	14.06-13.35	260.75	14.34	14.97-13.86	255.25	14.01	14.51-13.78
Ruppert Lake (20)	335.5	14.82	15.78-13.87	347.5	15.36	16.43-14.15	341.5	15.08	16.11-14.02
Xindi Lake (33)	191.5	14.28	16.50-13.49	209.5	15.63	18.06-14.77	200.5	15.00	18.18-13.59
Harding Lake (34)	333	13.32	14.48-12.42	348	14.24	15.73-12.97	340.5	13.78	15.12-12.70
Birch Lake (36)	1837	14.61	15.05-14.15	1842	14.73	15.17-14.26	1839.5	14.68	15.09-14.23
Lost Lake (22)	360	13.29	14.48-11.95	370	13.48	14.59-12.17	365	13.39	14.49-12.12
Jan Lake (23)	276	11.00	11.57-10.33	281	11.12	11.65-10.46	278.5	11.05	11.60-10.41
Idavain Lake (37)	870	13.87	14.08-13.59	890	13.98	14.25-13.79	880	13.93	14.14-13.78
Beaver Lake (38)	350	13.55	13.93-13.25	360	14.18	14.42-13.89	355	13.88	14.03-13.80
Discovery Pond (39)	420	13.92	14.47-13.43	423	14.13	14.83-13.51	421.5	14.03	14.66-13.46

SI References

1. P. M. Anderson, M. E. Edwards, L. B. Brubaker, Results and paleoclimate implications of 35 years of paleoecological research in Alaska. Developments in Quaternary Sciences 1, 427–440 (2004).
2. V. G. Goetcheus, H. H. Birks, Full-glacial upland tundra vegetation preserved under tephra in the Beringia National Park, Seward Peninsula, Alaska. Quaternary Science Reviews 20, 135–147 (2001).
3. G. D. Zazula, D. G. Froese, S. A. Elias, S. Kuzmina, R. W. Mathewes, Arctic ground squirrels of the mammoth steppe: paleoecology of Late Pleistocene middens (~24,000–29,450 14C yr BP), Yukon Territory, Canada. Quaternary Science Reviews 26, 979–1003 (2007).
4. M. E. Edwards, L. B. Brubaker, A. V. Lozhkin, P. M. Anderson, Structurally novel biomes: a response to past warming in Beringia. Ecology 86, 1696–1703 (2005).
5. M. B. Abbott, T.W. Stafford, Radiocarbon geochemistry of modern and ancient Arctic lake systems, Baffin Island, Canada. Quaternary Research 45, 300–311 (1996).
6. W. W. Oswald et al., Effects of sample mass and macrofossil type on radiocarbon dating of arctic and boreal lake sediments. The Holocene 15, 758–767 (2005).
7. B. V. Gaglioti et al., Radiocarbon age-offsets in an arctic lake reveal the long-term response of permafrost carbon to climate change. Journal of Geophysical Research: Biogeosciences 119, 1630–1651 (2014).
8. L. C. Cwynar, A Late-Quaternary Vegetation History from Hanging Lake, Northern Yukon: Ecological Archives M052-001. Ecological Monographs 52, 1–24 (1982).
9. J. Kurek, L. C. Cwynar, J. C. Vermaire, A late Quaternary paleotemperature record from Hanging Lake, northern Yukon Territory, eastern Beringia. Quaternary Research 72, 246–257 (2009).
10. F. S. Hu, L. B. Brubaker, P. M. Anderson, Postglacial vegetation and climate change in the northern Bristol Bay region, southwestern Alaska. Quaternary Research 43, 382–392 (1995).
11. F. S. Hu, A. Shemesh, A biogenic-silica δ18O record of climatic change during the last glacial–interglacial transition in southwestern Alaska. Quaternary Research 59, 379–385 (2003).
12. R. S. Anderson, E. Berg, C. Williams, T. Clark, Postglacial vegetation community change over an elevational gradient on the western Kenai Peninsula, Alaska: pollen records from Sunken Island and Choquette Lakes. Journal of Quaternary Science 34, 309–322 (2009).
13. B. V. Gaglioti et al., Younger-Dryas cooling and sea-ice feedbacks were prominent features of the Pleistocene-Holocene transition in Arctic Alaska. Quaternary Science Reviews 169, 330–343 (2017).
14. R. D. Guthrie, New carbon dates link climatic change with human colonization and Pleistocene extinctions. Nature 441, 207–209 (2006).
15. D. H. Mann, P. Groves, M. L. Kunz, R. E. Reanier, B. V. Gaglioti, B.V, Ice-age megafauna in Arctic Alaska: extinction, invasion, survival. Quaternary Science Reviews 70, 91–108 (2013).
16. R. E. LeResche, R. H. Bishop, J. W. Coady, Distribution and habitats of moose in Alaska. Naturaliste canadien 101, 143 (1974).
17. K. D. Tape, D. D. Gustine, R. W. Ruess, L. G. Adams, J. A. Clark, Range expansion of moose in Arctic Alaska linked to warming and increased shrub habitat. PloS one 11, p.e0152636 (2016)
18. J. Zhou et al., 2020. Enhanced shrub growth in the Arctic increases habitat connectivity for browsing herbivores. Global change biology 26, 3809–3820 (2020).
19. F. Irvine, L. C. Cwynar, J. C. Vermaire, A. B. Rees, 2012. Midge-inferred temperature reconstructions and vegetation change over the last ~15,000 years from Trout Lake, northern Yukon Territory, eastern Beringia. Journal of Paleolimnology 48, 133–146 (2012).
20. S. McGowan et al., Vegetation transitions drive the autotrophy–heterotrophy balance in Arctic lakes. Limnology and Oceanography Letters 3, 246–255 (2018).
21. W. W. Oswald, D. G. Gavin, P. M. Anderson, L. B. Brubaker, F. S. Hu, A 14,500-year record of landscape change from Okpilak Lake, northeastern Brooks Range, northern Alaska. Journal of paleolimnology 48, 101–113 (2012).
22. W. Tinner et al., Postglacial vegetational and fire history: pollen, plant macrofossil and charcoal records from two Alaskan lakes. Vegetation History and Archaeobotany 15, 279–293 (2006).

23. L. J. Carlson, B. P. Finney, A 13,000-year history of vegetation and environmental change at Jan Lake, east-central Alaska. The Holocene 14, 818–827 (2004).
24. C. Bronk Ramsey, Deposition models for chronological records. Quaternary Science Reviews 27, 42–60 (2008).
25. C. Bronk Ramsey, Bayesian analysis of radiocarbon dates. Radiocarbon 51, 337–360 (2009a).
26. C. Bronk Ramsey, S. Lee, Recent and planned developments of the program OxCal. Radiocarbon 55, 720–730 (2013).
27. P. J. Reimer et al., The IntCal20 northern hemisphere radiocarbon age calibration curve (0–55 cal kBP). Radiocarbon 62, 725–757 (2020).
28. C. Bronk Ramsey, Dealing with outliers and offsets in radiocarbon dating. Radiocarbon 51, 1023–1045 (2009b).
29. W. W. Oswald, L. B. Brubaker, P. M. Anderson, Late Quaternary vegetational history of the Howard Pass area, northwestern Alaska. Canadian Journal of Botany 77, 570–581 (1999).
30. M. B. Abbott, M. E. Edwards, B. P. Finney, A 40,000-yr record of environmental change from Burial Lake in Northwest Alaska. Quaternary Research 74, 156–165 (2010).
31. A. Monteath et al., Chronology and glass chemistry of tephra and cryptotephra horizons from lake sediments in northern Alaska, USA. Quaternary Research 88, 169–178 (2017).
32. L. J. Davies, B. J. Jensen, D. G. Froese, K. L. Wallace, Late Pleistocene and Holocene tephrostratigraphy of interior Alaska and Yukon: Key beds and chronologies over the past 30,000 years. Quaternary Science Reviews 146, 28–53 (2016).
33. P. E. Higuera, et al., Frequent fires in ancient shrub tundra: implications of paleorecords for arctic environmental change. PloS one 3, p.e0001744 (2008).
34. M. S. Finkenbinder et al,, A 31,000 year record of paleoenvironmental and lake-level change from Harding Lake, Alaska, USA. Quaternary Science Reviews 87, 98–113 (2014).
35. M. S. Finkenbinder, M. B. Abbott, B. P. Finney, J. S. Stoner, J. M. Dorfman, A multi-proxy reconstruction of environmental change spanning the last 37,000 years from Burial Lake, Arctic Alaska. Quaternary Science Reviews 126, 227–241 (2015).
36. N. H. Bigelow, “Late Quaternary vegetation and lake level changes in central Alaska, PhD thesis”, University of Alaska Fairbanks (1997).
37. L. B. Brubaker, P. M. Anderson, F. S. Hu, Vegetation ecotone dynamics in southwest Alaska during the late Quaternary. Quaternary Science Reviews 20, 175–188 (2001).
38. P. Kaltenrieder, W. Tinner, B. Lee, F. S. Hu, 2011. A 16,000-year record of vegetational change in south-western Alaska as inferred from plant macrofossils and pollen. Journal of Quaternary Science 26, 276–285 (2011).
39. D. S. Kaufman, R. S. Anderson, F. S. Hu, E. Berg, A. Werner, Evidence for a variable and wet Younger Dryas in southern Alaska. Quaternary Science Reviews 29, 1445–1452 (2010).
40. D. H. Mann, D. M. Peteet, R. E. Reanier, M. L. Kunz, Responses of an arctic landscape to Lateglacial and early Holocene climatic changes: the importance of moisture. Quaternary Science Reviews 21, 997–1021 (2002).
41. N. H. Bigelow, M. E. Edwards, A 14,000 yr paleoenvironmental record from Windmill Lake, central Alaska: Lateglacial and Holocene vegetation in the Alaska Range. Quaternary Science Reviews 20, 203–215 (2001).
42. F. S. Hu, B. Y. Lee, D. S. Kaufman, S. Yoneji, D. M. Nelson, P. D. Henne, Response of tundra ecosystem in southwestern Alaska to Younger-Dryas climatic oscillation. Global Change Biology 8, 1156–1163 (2002).
43. F. S. Hu et al., Abrupt climatic events during the last glacial-interglacial transition in Alaska. Geophysical Research Letters 33 (2006).
44. M. Fritz et al., Late glacial and Holocene sedimentation, vegetation, and climate history from easternmost Beringia (northern Yukon Territory, Canada). Quaternary Research 78, 549-560 (2012).

45. J. C. Vermaire, L. C. Cwynar, A revised late-Quaternary vegetation history of the unglaciated southwestern Yukon Territory, Canada, from Antifreeze and Eikland ponds. Canadian Journal of Earth Sciences 47, 75–88 (2010).
46. S. O. Rasmussen et al., A new Greenland ice core chronology for the last glacial termination. Journal of Geophysical Research: Atmospheres 111 (2006).
47. C. Bronk Ramsey, Methods for summarizing radiocarbon datasets. Radiocarbon 59, 1809–1833 (2017).